

Active Brownian Motion in Two Dimensions

Urna Basu,^{1,2} Satya N. Majumdar,¹ Alberto Rosso,¹ and Grégory Schehr¹

¹*LPTMS, CNRS, Univ. Paris-Sud, Université Paris-Saclay, 91405 Orsay, France*

²*Raman Research Institute, Bangalore 560080, India*

We study the dynamics of a single active Brownian particle (ABP) in two spatial dimensions. The ABP has an intrinsic time scale D_R^{-1} set by the rotational diffusion constant D_R . We show that, at short-times $t \ll D_R^{-1}$, the presence of ‘activeness’ results in a strongly anisotropic and non-diffusive dynamics in the (xy) plane. We compute exactly the marginal distributions of the x and y position coordinates along with the radial distribution, which are all shown to be non-Brownian. In addition, we show that, at early times, the ABP has anomalous first-passage properties, characterized by non-Brownian exponents.

I. INTRODUCTION

Active particles form a class of nonequilibrium systems which are able to generate dissipative directed motion through self-propulsion and consuming energy from their environment [1–6]. Study of active particles is relevant in a wide variety of biological and soft matter systems ranging from bacterial motion [7, 8], cellular tissue behavior [9], formation of fish schools [10, 11] as well as granular matter [12, 13] and colloidal surfers [14]. Recent years have seen a tremendous surge of research, both theoretical and experimental, on active matter e.g., the collective behavior of active particles which include flocking [15, 16], clustering [14, 17, 18], phase separation [19–21] and the absence of a well defined pressure [22].

Remarkably, even at a single particle level, active particles show many interesting features like anomalous dynamical behavior [23–25], non-Boltzmann stationary distribution [24–30] and accumulation near confining boundaries [31–33]. One of the simplest and most extensively studied models of active particles is the so called active Brownian particle (ABP) [3, 5, 34–36] which describes directed spatial motion of overdamped particles at a fixed speed with the direction performing a rotational diffusion, with diffusion constant D_R . Interestingly, the same model was also studied as a toy model of computer vision [37], as well as in reaction-diffusion systems [38]. Despite the apparent simplicity of the model, an exact analytical description of the dynamics, beyond the mean-squared radial displacement [3, 39, 40], is unfortunately still lacking.

The diffusion of the rotational degree of freedom sets a time scale D_R^{-1} which characterizes the persistence of the direction for an ABP. At very late times, one indeed recovers Brownian diffusion with an effective diffusion constant [3, 5]. However, this effective Brownian picture does not hold at short times where memory effects are important. In this Letter, we show that at *short times* the ABP exhibits a strikingly different behavior compared to the ordinary Brownian motion, with clear fingerprints of ‘activeness’ of the motion. For a given initial orientation of the velocity, we show that at short-times the dynamics is highly anisotropic, with the typical displacements along and transverse to the initial orientation scaling very

differently with time. The corresponding distributions turn out to be strongly non-Brownian in nature. We compute exactly these marginal position distributions at short times using path-integral techniques for Brownian functionals. We show that, at short times, the dynamics transverse to the initial orientation can be mapped to the ‘Random Acceleration Process’ (RAP) [41–47], a well studied non-Markovian process. Consequently, we show that the ABP exhibits anomalous first-passage properties at short times, with an associated nontrivial exponent in the transverse direction.

II. MODEL

We consider an active overdamped particle in the $2d$ -plane moving with a constant speed v_0 . In addition to its position coordinates (x, y) the particle has an ‘active’ internal degree of freedom, given by the orientational angle $\phi(t)$ of its velocity, which undergoes rotational diffusion. The time evolution is encoded in the Langevin equation [3–5]

$$\dot{x} = v_0 \cos \phi(t) \quad (1a)$$

$$\dot{y} = v_0 \sin \phi(t) \quad (1b)$$

$$\dot{\phi} = \sqrt{2D_R} \eta_\phi(t). \quad (1c)$$

Here $\eta_\phi(t)$ is a Gaussian white noise with zero mean and correlator $\langle \eta_\phi(t) \eta_\phi(t') \rangle = \delta(t - t')$ and D_R is the associated rotational diffusion constant. The ‘activeness’ in this model stems from the velocity in the x and y directions that are coupled to the orientation $\phi(t)$. This is in contrast to the standard Brownian motion (SBM) where the x and y coordinates undergo uncorrelated translational diffusion with some diffusion constant D : $\dot{x} = \sqrt{2D} \eta_x(t)$, $\dot{y} = \sqrt{2D} \eta_y(t)$ where $\eta_{x,y}(t)$ are independent delta-correlated white noises.

The Langevin equations (1) can be cast in a form similar to that of ordinary Brownian motion where $\xi_x(t) = v_0 \cos \phi(t)$ and $\xi_y(t) = v_0 \sin \phi(t)$ are the effective noises acting on the ABP. However, these ‘active’ effective noises differ from the usual white-noise on two crucial aspects. First, their magnitude is bounded with $\xi_x(t) \leq v_0$ (and similarly for $\xi_y(t)$) at all times t . Secondly, both

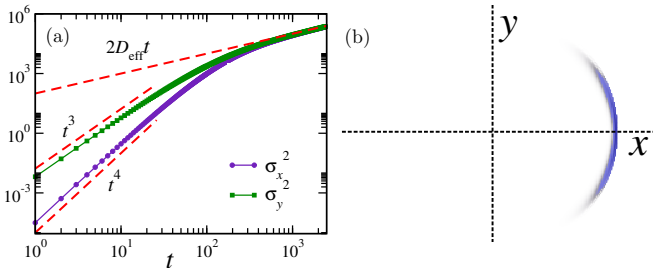


FIG. 1: (a) Mean-squared displacement $\sigma_{x,y}^2$ of x and y components of the position of an ABP as a function of t for $v_0 = 1$ and $D_R = 0.01$. The symbols correspond to simulations and the solid lines are the predictions from the exact calculations. (b) Position probability distribution $P(x, y, t)$ in the (xy) plane for $D_R = 0.1$ and $v_0 = 1$ at an early time $t = 1$.

$\xi_x(t)$ and $\xi_y(t)$ have an auto-correlation function which decays exponentially for large t_1, t_2 ,

$$\langle \xi_x(t_1)\xi_x(t_2) \rangle \simeq \frac{v_0^2}{2} \exp[-D_R|t_1 - t_2|] \quad (2)$$

and similarly for $\xi_y(t)$ [see Appendix A for details]. Moreover, ξ_x and ξ_y are also mutually correlated which makes x and y -coordinates correlated in ABP, in contrast to the SBM. Clearly, for times $t \gg D_R^{-1}$, the noise correlation in (2) converges to $\langle \xi_x(t_1)\xi_x(t_2) \rangle \rightarrow 2D_{\text{eff}}\delta(t_1 - t_2)$ with an effective diffusion constant $D_{\text{eff}} = v_0^2/(2D_R)$. Hence, for $t \gg D_R^{-1}$, ABP effectively reduces to the SBM [3, 5]. However, at short-times, the effective noise $\xi_x(t)$ (and $\xi_y(t)$) is correlated in time [see Eq. (2)] and we expect memory effects to be important, giving rise to a strong signature of ‘activeness’.

III. SHORT-TIME REGIME

Consider an ABP starting initially at the origin $x = y = 0$ with a given orientation, which we choose, without any loss of generality, to be along the x -axis, so that $\phi(0) = 0$. The initial value of $\phi(0)$ selects a specific direction (x here), thereby breaking the symmetry between the dynamics of the x and the y coordinates in Eqs. (1a) and (1b). The simplest observable that shows this anisotropy is the mean-squared displacement (MSD) for the x and the y coordinates separately. In fact, the radial MSD in this model $\langle r^2 \rangle = \langle x^2 \rangle + \langle y^2 \rangle$ was computed long time back [3, 39, 40]. However, to investigate the anisotropy, we need to compute the x -MSD $\sigma_x^2 = \langle x^2 \rangle - \langle x \rangle^2$ and y -MSD $\sigma_y^2 = \langle y^2 \rangle - \langle y \rangle^2$ separately. Indeed, in Eq. (C4) of Appendix C we show that σ_x^2 and σ_y^2 can be computed exactly at all times t . From this

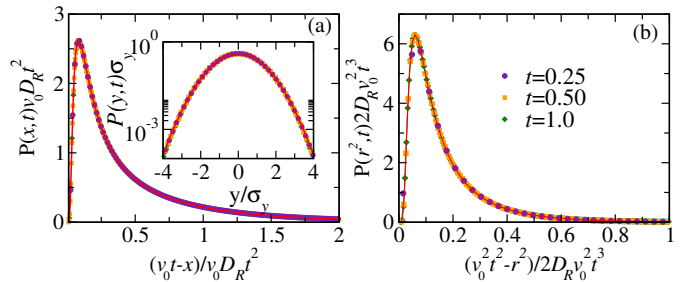


FIG. 2: Marginal distributions $P(x, t)$ (a), $P(y, t)$ (inset of (a)) and $P(r^2, t)$ (b) in the short-time regime for different values of $t \ll D_R^{-1}$ for $D_R = 0.01$ and $v_0 = 1$. The data are scaled according to the scaling forms predicted in the text and compared with the exact results computed therein.

exact result, the small $t \ll D_R^{-1}$ behavior can be read off,

$$\sigma_x^2 \approx \frac{1}{3}v_0^2 D_R^2 t^4 - \frac{7}{15}v_0^2 D_R^3 t^5 + \dots \quad (3)$$

$$\sigma_y^2 \approx \frac{2}{3}v_0^2 D_R t^3 - \frac{5}{6}v_0^2 D_R^2 t^4 + \dots, \quad (4)$$

manifesting clearly the anisotropy, as well as the non-diffusive behavior at short times. Evidently, for small t , the MSD in the x -direction $\sigma_x^2 \sim t^4$ is much smaller than that in the y -direction $\sigma_y^2 \sim t^3$. This is in clear contrast to a SBM where the mean-squared displacements $\sim t$ at all times, and in both x and y directions. Figure 1 compares the exact result of Eq. (C4) of Appendix C (solid lines) with the $\sigma_{x,y}^2$ obtained from simulations (symbols). As discussed before, at late times $t \gg D_R^{-1}$, both $\sigma_{x,y}^2 \approx 2Dt$ behave diffusively with $D_{\text{eff}} = v_0^2/2D_R$ [see Eq. (C4) of Appendix C].

To further characterize the anisotropic and non-diffusive early time behavior of ABP, we compute the position probability distribution function (PDF) $P(x, y, t)$. Figure 1(b) shows $P(x, y, t)$ in the (x, y) plane for $t \ll D_R^{-1}$, obtained from numerical simulations of ABP. The PDF for ABP, at early times, has an anisotropic ‘sickle-like’ shape, with a peak near $x = v_0 t$ and $y = 0$. This is in clear contrast to the passive case where the PDF has a Gaussian (isotropic) shape with a peak at the origin.

The position PDF can, in principle, be obtained by integrating over the orientational degree of freedom, i.e., $P(x, y, t) = \int_{-\infty}^{\infty} \mathcal{P}(x, y, \phi, t) d\phi$, where $\mathcal{P}(x, y, \phi, t)$ satisfies a Fokker-Planck (FP) equation (see Eq. (B1) in Appendix B). Unfortunately, this FP equation is hard to solve at all times [37]. However, in the short-time regime, analytical progress can be made by using path-integral method for Brownian functionals [48]. In this limit, $\phi(t) \sim \sqrt{t}$ is small, and Eqs. (1a) and (1b) can be approximated by $\dot{x} \approx v_0(1 - \frac{1}{2}\phi^2(t))$ and $\dot{y} \approx v_0\phi(t)$, keeping terms up to $\mathcal{O}(\phi^2(t))$ in the expansions of $\cos \phi(t)$ and $\sin \phi(t)$.

It is useful to write $\phi(t) = \sqrt{2D_R}B(t)$ where $B(t)$ is the SBM. Using the scaling property of Brownian motion $B(at) = \sqrt{a}B(t)$, the x and the y coordinates can be

expressed as

$$\begin{aligned} x(t) &= v_0 t - v_0 D_R t^2 \int_0^1 ds B^2(s) \\ y(t) &= v_0 \sqrt{2D_R} t^{3/2} \int_0^1 ds B(s). \end{aligned} \quad (5)$$

The position PDF then takes the scaling form

$$P(x, y, t) = \frac{1}{\sqrt{2}v_0^2 D_R^{3/2} t^{7/2}} \tilde{P}\left(\frac{v_0 t - x}{v_0 D_R t^2}, \frac{y}{v_0 \sqrt{2D_R} t^{3/2}}\right), \quad (6)$$

where $\tilde{P}(a_1, a_2)$ is the joint-distribution of the two (correlated) Brownian functionals,

$$a_1 = \int_0^1 B^2(s) ds, \quad \text{and} \quad a_2 = \int_0^1 B(s) ds. \quad (7)$$

We calculate the double Laplace transform of $\tilde{P}(a_1, a_2)$ using path-integral approach [see Appendix D for details], and get

$$\langle \exp[-\lambda_1 a_1 - \lambda_2 a_2] \rangle = \frac{\exp[\lambda_2^2 C(\lambda_1)]}{\sqrt{\cosh(\sqrt{2}\lambda_1)}} \quad (8)$$

where $C(\lambda_1) = \frac{1}{4\lambda_1} \left[1 - \frac{\tanh(\sqrt{2}\lambda_1)}{\sqrt{2}\lambda_1}\right]$. The scaling function $\tilde{P}(a_1, a_2)$ (and hence the PDF $P(x, y, t)$) can, in principle, be obtained by inverting the double Laplace transform in Eq. (8). Unfortunately, this inversion is difficult. Nevertheless, useful informations can still be extracted from this Laplace transform as we show below.

Integrating Eq. (6) over y , the marginal distribution of x clearly has the scaling form

$$P(x, t) = \frac{1}{v_0 D_R t^2} f_x\left(\frac{v_0 t - x}{v_0 D_R t^2}\right), \quad (9)$$

where $f_x(a_1)$ is the PDF of a_1 defined in Eq. (7). The Laplace transform of $f_x(a_1)$ is obtained from Eq. (8) by setting $\lambda_2 = 0$,

$$\langle e^{-\lambda_1 a_1} \rangle = \int_0^\infty e^{-\lambda_1 a_1} f_x(a_1) da_1 = \frac{1}{\sqrt{\cosh(\sqrt{2}\lambda_1)}}. \quad (10)$$

This Laplace transform can now be explicitly inverted (see Appendix E) to give

$$f_x(a_1) = \frac{1}{2\sqrt{\pi a_1^3}} \sum_{k=0}^{\infty} (-1)^k \frac{(4k+1)}{2^{2k}} \binom{2k}{k} e^{-\frac{(4k+1)^2}{8a_1}}, \quad (11)$$

for $a_1 \geq 0$. The scaling function $f_x(a_1)$ is manifestly non-Gaussian with the asymptotic behaviors (see Appendix E): $f_x(a_1) \simeq \frac{1}{2\sqrt{\pi a_1^3}} e^{-\frac{1}{8a_1}}$ as $a_1 \rightarrow 0$ and $f_x(a_1) \simeq \frac{1}{\sqrt{2a_1}} e^{-\frac{\pi^2 a_1}{8}}$ as $a_1 \rightarrow \infty$. This function has a peak close to $a_1 = 0$, which corresponds to $x \approx v_0 t$ [see Fig. 2(a)] and it decays exponentially fast away from the edge, i.e.

for $x \ll v_0 t$. In Fig. 2(a) we compare the exact result (solid line) and the data obtained from numerical simulations for different values of $t \ll D_R^{-1}$ for a fixed D_R . The excellent agreement confirms the scaling form (9) along with the analytical prediction Eq. (11) for $t \ll D_R^{-1}$.

The marginal distribution for the y -component, on the other hand, takes a very different form. Taking the limit $\lambda_1 \rightarrow 0$ in Eq. (8) we get the Laplace transform $\langle \exp[-\lambda_2 a_2] \rangle = \exp[\lambda_2^2/6]$. Upon Laplace inversion, $P(y, t)$ has a pure Gaussian form, $P(y, t) = \exp[-y^2/2\sigma_y^2]/\sqrt{2\pi\sigma_y^2}$ with the variance $\sigma_y^2 = 2v_0^2 D_R t^3/3$, consistent with the first term in Eq. (4). The inset of Fig. 2(a) shows $P(y, t)$ for different values of $t \ll D_R^{-1}$ as a function of y/σ_y compared to the Gaussian (solid line), verifying the analytical prediction.

For a 2d SBM with diffusion constant D , the x and y coordinates are completely independent (each of them is a 1d Brownian motion), and hence the position PDF in the (xy) plane is simply $P(x, y, t) = e^{-(x^2+y^2)/(4Dt)}/(4\pi Dt)$. Hence it is isotropic in the (xy) plane and in particular the PDF of $r^2 = x^2 + y^2$ is simply $P(r^2, t) = e^{-r^2/(4Dt)}/(4Dt)$. In contrast, for an ABP, the x and y coordinates are strongly correlated at short times and hence we expect a different behavior for $P(r^2, t)$. Indeed, this PDF $P(r^2, t)$ can also be computed explicitly by exploiting the result in Eq. (8). From Eq. (5), we have $r^2 = x^2 + y^2 \simeq v_0^2 t^2 - 2D_R v_0^2 t^3 (a_1 - a_2^2)$ up to order $\mathcal{O}(t^3)$, where a_1 and a_2 are given in Eq. (7). Thus $P(r^2, t)$, for $t \ll D_R^{-1}$, is expected to behave as

$$P(r^2, t) = \frac{1}{2D_R v_0^2 t^3} f_r\left(\frac{v_0^2 t^2 - r^2}{2D_R v_0^2 t^3}\right) \quad (12)$$

where $f_r(z)$ is the probability distribution of $z = a_1 - a_2^2$. Its Laplace transform can be extracted from Eq. (8) after a few steps of algebra detailed in Appendix G,

$$\langle e^{-\lambda z} \rangle = \int_0^\infty e^{-\lambda z} f_r(z) dz = \left[\frac{\sqrt{2\lambda}}{\sinh(\sqrt{2}\lambda)} \right]^{1/2}, \quad (13)$$

which, fortunately, can be inverted explicitly. The resulting expression, given in Eq. (G14) in Appendix G, is somewhat long but explicit. It has the asymptotic behaviors: $f_r(z) \simeq \frac{1}{2\sqrt{2\pi z^2}} e^{-1/(8z)}$ as $z \rightarrow 0$ and $f_r(z) \simeq \sqrt{\frac{\pi}{z}} e^{-\pi^2 z/2}$ as $z \rightarrow \infty$. This scaling function $f_r(z)$ is plotted and compared to simulations in Fig. 2(b) with excellent agreement.

Let us remark that this radial distribution $P(r^2, t)$ in Eq. (12), being an average over the angular degree, does not provide any information about the anisotropy present in the (xy) plane. It just demonstrates that the strong correlations between the x and y coordinates at short times make the radial distribution very different from that of the SBM case. Even if one averages over the initial orientation angle $\phi(0)$ uniformly over $[0, 2\pi]$, thus restoring isotropy in the (xy) plane at all times, $P(r^2, t)$ is still given by the same expression as in (12),

which manifestly is still different from the SBM. This rotationally symmetric case was qualitatively discussed in Ref. [40, 49], although no analytical form for the distribution was found. Very recently, the Fourier transform of the PDF was computed as a formal eigenfunctions expansion in terms of the Mathieu functions [50]. However, inverting this formal Fourier transform and plotting it in real space is still highly difficult. Our approach provides an explicit real space distribution, which is exact at short times.

IV. FIRST-PASSAGE PROPERTIES

The discussion above clearly shows a crossover from early time, non-diffusive and anisotropic behavior (a fingerprint of ‘activeness’) to the late time diffusive and isotropic Brownian behavior, at a crossover time $t \sim D_R^{-1}$. Another natural observable that demonstrates this crossover in a candid way is the first-passage probability. In fact, for active systems, the first-passage properties have not been explored much, except very recently in a class of one-dimensional models [23, 51–53]. The first-passage probability is most conveniently defined through the survival probability [41, 42, 54]. Let us start with the x -coordinate and denote by $S_x(t; x_0)$ the probability that the x -component, starting at $x_0 \geq 0$, does not cross $x = 0$ up to time t (clearly it does not depend on y). The associated first-passage probability is just $-\partial_t S_x(t; x_0)$. In this case, at early times $t \ll D_R^{-1}$, $x(t) \approx v_0 t$ with $v_0 > 0$, as in Eq. (5), and therefore $x(t)$ stays positive with probability close to unity. However, at long times $t \gg D_R^{-1}$, $x(t)$ behaves diffusively and we would expect [41, 42, 54] a decay $\sim t^{-1/2}$ of $S_x(t; x_0)$ at late times. For simplicity, we set $x_0 \rightarrow 0$ and in this case, we naturally expect a crossover behavior of the form

$$S_x(t; x_0 \rightarrow 0) = \mathcal{F}_x(t D_R) , \quad (14)$$

where the crossover function $\mathcal{F}_x(u) \sim 1$ for $u \ll 1$, while $\mathcal{F}_x(u) \sim u^{-1/2}$ for $u \gg 1$. Figures 3(a) and (b) show the behavior of $S_x(t; x_0 \rightarrow 0)$ for different values of D_R . The collapsed data in Fig. 3(b) are in agreement with the proposed scaling form in Eq. (14).

We expect the first-passage probability for the y -coordinate to be rather different due to the anisotropy present in early times. As in the x -case, we denote by $S_y(t; y_0)$ the survival probability that the y -coordinate, starting initially at $y_0 > 0$, stays positive up to time t . At times $t \ll D_R^{-1}$, the effective Langevin equation for the y -coordinate, $\dot{y} \approx v_0 \phi(t)$, can be recast (after taking one more time-derivative) as

$$\ddot{y} \approx \sqrt{2 D_{\text{RAP}}} \eta_\phi(t) , \quad \text{where } D_{\text{RAP}} = v_0^2 D_R . \quad (15)$$

This effective Langevin equation for the y -coordinate is thus exactly identical to the celebrated ‘Random Acceleration Process’ (RAP), which has been studied extensively in the literature as one of the simplest non-Markovian processes (see [41–45]). One hallmark of this

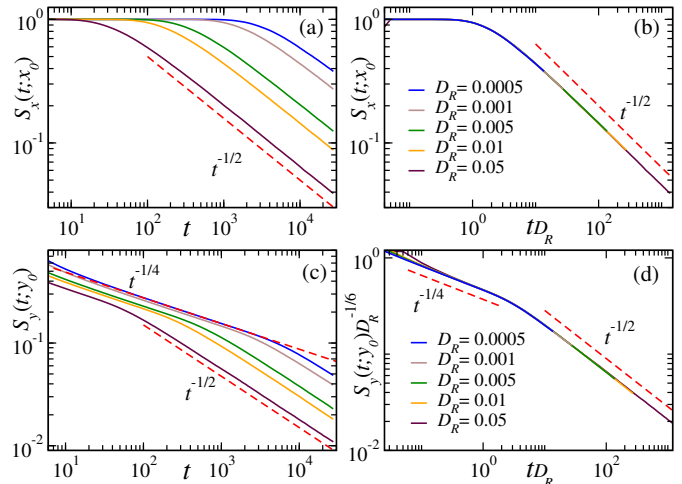


FIG. 3: Survival probability: (a) Plot of $S_x(t; x_0)$ as a function of time t for different values of D_R and the initial position $x_0 = 0.1, y_0 = 0$. (b) Collapse of the curves in (a) following Eq. (14). (c) $S_y(t; y_0)$ vs t for different values of D_R and the initial position $x_0 = 0, y_0 = 0.1$. The curves initially show a power law decay $t^{-1/4}$ which crosses over to $t^{-1/2}$ after a time $t \sim D_R^{-1}$. The topmost dashed line is the exact prediction from the RAP in Eq. (16). (d) Collapse of the curves in (c) according to Eq. (17). Here $v_0 = 1$ for all the curves.

non-Markovian nature is an anomalously slow decay of the survival probability $S_y(t; y_0) \sim t^{-1/4}$ (for $t \gg 1$) [41–44, 46], in marked contrast to the $t^{-1/2}$ decay of the SBM [41, 42, 54]. In the limit $y_0 \rightarrow 0$, the full survival probability (and not just the persistence exponent 1/4) can be computed [47]. Translating this result in our units we then predict, for $t \gg 1$

$$S_y(t; y_0) \simeq \frac{2^{5/6} \Gamma(-4/3)}{3^{2/3} \pi \Gamma(3/4)} \left(\frac{y_0 D_R}{v_0} \right)^{1/6} (t D_R)^{-1/4} . \quad (16)$$

Since the mapping to the RAP holds only for $t \ll D_R^{-1}$, we expect this result in (16) to hold for $1 \ll t \ll D_R^{-1}$. For $t \gg D_R^{-1}$, given that the ABP behaves as a SBM, we would expect $S_y(t; y_0)$ to decay as $t^{-1/2}$. This suggests a crossover from the early time $\sim t^{-1/4}$ to the late time $t^{-1/2}$ decay of $S_y(t; y_0)$, described by the scaling form

$$S_y(t; y_0) = \left(\frac{y_0 D_R}{v_0} \right)^{1/6} \mathcal{F}_y(t D_R) , \quad (17)$$

where the crossover scaling function $\mathcal{F}_y(u)$ has the limiting behaviors: $\mathcal{F}_y(u) \sim u^{-1/4}$ for $u \ll 1$ and $\mathcal{F}_y(u) \sim u^{-1/2}$ for $u \gg 1$. We have verified this scaling form (17) numerically. Figure 3(c) shows $S_y(t; y_0)$ vs. t , obtained from simulations, for different values of D_R . The uppermost dashed line in Fig. 3(c) is the exact prediction from Eq. (16). The same data scaled according to Eq. (17) are plotted in Fig 3(d). The excellent data collapse confirms the predicted scaling form (17).

V. CONCLUSION

We have studied the dynamics of an ABP in $2d$. The rotational diffusion sets a timescale D_R^{-1} for the dynamics of the spatial coordinates of the ABP. While for $t \gg D_R^{-1}$ the ABP reduces to an ordinary $2d$ Brownian motion, we have shown that the fingerprint of the ‘activeness’ of motion shows up for $t \ll D_R^{-1}$, where the dynamics is highly anisotropic with strong correlations between the x and the y -coordinates. For short times, we have computed exactly the marginal distributions $P(x, t)$, $P(y, t)$ as well as the radial marginal distribution $P(r^2, t)$, well verified by numerical simulations. In addition, we have shown that, at these early times, the ABP has anomalous first-passage properties. In particular, the survival probability in the y -direction decays anomalously as $t^{-1/4}$ for $1 \ll t \ll D_R^{-1}$.

An alternative way to explore the anomalous ‘active’ behavior is to apply an external confining potential such as a harmonic trap $V(r) = \mu r^2/2$, that introduces an additional time scale μ^{-1} . By tuning μ , one can show that the anomalous early time fingerprints of the free ABP studied here can be made to persist even at late times, leading to non-Boltzmann stationary states [55]. Indeed, a crossover from Boltzmann (passive) to non-Boltzmann (active) stationary states in the presence of a trap has been studied using numerical simulations and scaling arguments [35, 36], as well as in recent experiments on trapped self-propelled particles [56, 58]. By tuning these two timescales, D_R^{-1} and μ^{-1} , it would be interesting to see if our analytical predictions at short times for the free ABP can be observed experimentally.

Acknowledgments

The authors would like to acknowledge the support from the Indo-French Centre for the promotion of advanced research (IFCPAR) under Project No. 5604-2. We thank I. Dornic and J. M. Luck for useful discussions and for pointing out Ref. [37]. We would also like to thank ICERM for hospitality, where part of this work has been done.

Appendix A: Effective Noise

The Langevin equation (1) reads

$$\begin{aligned} \dot{x} &= v_0 \cos \phi(t) = \xi_x(t) \\ \dot{y} &= v_0 \sin \phi(t) = \xi_y(t) \end{aligned} \quad (\text{A1})$$

where $\xi_x(t)$ and $\xi_y(t)$ are the effective noises in the x and the y direction respectively. Here, $\phi(t)$ is a Brownian motion with a diffusion constant D_R [see Eq. (1) in the main text] starting from $\phi(0) = 0$. Clearly, $\phi(t)$ is a Gaussian process with two-point correlation

$$\langle \phi(t_1)\phi(t_2) \rangle = 2D_R \min(t_1, t_2). \quad (\text{A2})$$

The noise $\xi_{x,y}(t)$ are bounded in time, even though $\phi(t)$ grows with time as $\phi(t) \sim \sqrt{2D_R t}$. It is convenient to use the exponential forms for the noise, $\xi_x(t) = \frac{1}{2}(e^{i\phi(t)} + e^{-i\phi(t)})$ and $\xi_y(t) = \frac{1}{2i}(e^{i\phi(t)} - e^{-i\phi(t)})$. The one and two-point correlation functions of the noise $\xi_{x,y}(t)$ can then be computed using the fact that $\phi(t)$ is a Gaussian process. In fact, we will use a well known identity for a Gaussian process $\phi(t)$,

$$\left\langle \exp \left(i \sum_j b_j \phi(t_j) \right) \right\rangle = \exp \left(-\frac{1}{2} \sum_{j,k} b_j b_k \langle \phi(t_j)\phi(t_k) \rangle \right) \quad (\text{A3})$$

where b_i ’s are arbitrary. The average values are thus given by

$$\langle \xi_x(t) \rangle = v_0 e^{-D_R t}, \langle \xi_y(t) \rangle = 0 \quad (\text{A4})$$

where we used Eq. (A3) with appropriate values of b_1 (and $t_1 = t$) and $b_j = 0$ for $j > 1$ and $\langle \phi^2(t) \rangle = 2D_R t$. Similarly the two-point functions can be obtained in a straightforward manner from Eq. (A3) by appropriately choosing b_1 and b_2 and keeping $b_j = 0$ for $j > 2$. We get

$$\langle \xi_x(t_1)\xi_x(t_2) \rangle = \frac{v_0^2}{2} \left[e^{-D_R|t_1-t_2|} + e^{-D_R(t_1+t_2+2\min(t_1,t_2))} \right]. \quad (\text{A5})$$

In the limit of $t_1 \rightarrow \infty, t_2 \rightarrow \infty$ but finite $|t_1 - t_2|$ the above expression reduces to Eq. (2) of the main text. The autocorrelation of $\xi_y(t)$ can also be computed similarly, yielding

$$\langle \xi_y(t_1)\xi_y(t_2) \rangle = \frac{v_0^2}{2} \left[e^{-D_R|t_1-t_2|} - e^{-D_R(t_1+t_2+2\min(t_1,t_2))} \right] \quad (\text{A6})$$

which has the same limiting behavior as the correlator of ξ_x for large t_1, t_2 (see Eq. (2) in the main text). The mutual two-point correlation $\langle \xi_x(t_1)\xi_y(t_2) \rangle$ vanishes due to symmetry, however, higher order mutual correlations remain finite. This is easily seen from the exact relation $\xi_x^2(t) + \xi_y^2(t) = v_0^2$, using Eq. (A1). From Eqs. (A5) and (A6) one sees that the effective noises $\xi_{x,y}(t)$ appearing in the Langevin equation (A1), have a finite correlation time D_R^{-1} , indicating that they have a finite memory.

Appendix B: Fokker-Planck Equation

Let $\mathcal{P}(x, y, \phi, t)$ denote the probability that at any time t , the ABP has a position (x, y) and orientation ϕ . $\mathcal{P}(x, y, \phi, t)$ evolves according to a Fokker-Planck equation,

$$\partial_t \mathcal{P}(x, y, \phi; t) = -v_0 \left[\cos \phi \frac{\partial \mathcal{P}}{\partial x} + \sin \phi \frac{\partial \mathcal{P}}{\partial y} \right] + D_R \frac{\partial^2 \mathcal{P}}{\partial \phi^2} \quad (\text{B1})$$

where we have suppressed the argument of \mathcal{P} on the right hand side for brevity. The marginal probability distribution of the position can then be obtained by integrating over ϕ ,

$$P(x, y, t) = \int_{-\infty}^{\infty} d\phi \mathcal{P}(x, y, \phi, t). \quad (\text{B2})$$

Appendix C: Mean-squared displacements

The mean-squared displacement (MSD) of the ABP can be exactly calculated from the Langevin equation (A1). The average displacements along the x and y directions immediately follow from (A4)

$$\langle x(t) \rangle = \int_0^t ds \langle \xi_x(s) \rangle = \frac{v_0}{D_R} (1 - e^{-D_R t}) \quad (\text{C1})$$

$$\langle y(t) \rangle = \int_0^t ds \langle \xi_y(s) \rangle = 0. \quad (\text{C2})$$

The computation of second moments involves the noise-correlators given in Eqs. (A5) and (A6),

$$\begin{aligned} \langle x^2(t) \rangle &= \int_0^t ds_1 \int_0^t ds_2 \langle \xi_x(s_1) \xi_x(s_2) \rangle \\ \langle y^2(t) \rangle &= \int_0^t ds_1 \int_0^t ds_2 \langle \xi_y(s_1) \xi_y(s_2) \rangle. \end{aligned} \quad (\text{C3})$$

Evaluating the above integrals, we get the variances of the x and the y -components separately,

$$\begin{aligned} \sigma_x^2 &= \langle x^2 \rangle - \langle x \rangle^2 \\ &= \frac{v_0^2}{D_R} t + \frac{v_0^2}{12D_R^2} [e^{-4D_R t} - 12e^{-2D_R t} + 32e^{-D_R t} - 21] \\ \sigma_y^2 &= \langle y^2 \rangle \\ &= \frac{v_0^2}{D_R} t - \frac{v_0^2}{12D_R^2} [e^{-4D_R t} - 16e^{-D_R t} + 15]. \end{aligned} \quad (\text{C4})$$

At long times $t \gg D_R^{-1}$, both $\sigma_x^2 \approx 2D_{\text{eff}} t$ and $\sigma_y^2 \approx 2D_{\text{eff}} t$ grow linearly with time with an effective diffusion constant $D_{\text{eff}} = v_0^2/(2D_R)$. In contrast, at short-times $t \ll D_R^{-1}$, expanding (C4) in Taylor series, we find

$$\sigma_x^2 \approx \frac{1}{3} v_0^2 D_R^2 t^3 - \frac{7}{15} v_0^2 D_R^3 t^5 + \dots$$

$$\sigma_y^2 \approx \frac{2}{3} v_0^2 D_R t^3 - \frac{5}{6} v_0^2 D_R^2 t^4 + \dots \quad (\text{C5})$$

which gives the results in Eqs. (3) and (4) of the main text. These results reflect a strong anisotropy at early times in the (x, y) plane since, for small t , $\sigma_x^2 \sim t^3 \gg \sigma_y^2 \sim t^4$.

Note that, from these results above, we can also compute the radial mean-squared displacement, defined as

$$\langle r^2(t) \rangle = \langle x^2(t) \rangle + \langle y^2(t) \rangle = \sigma_x^2 + \langle x \rangle^2 + \sigma_y^2. \quad (\text{C6})$$

Using the results from Eqs. (C1) and (C4) this gives

$$\langle r^2(t) \rangle = \frac{2v_0^2}{D_R} t + \frac{2v_0^2}{D_R^2} (e^{-D_R t} - 1). \quad (\text{C7})$$

This result for the radial MSD was in fact known for a long time [3]. However, the individual variances along the x and the y directions in Eq. (C4), which clearly illustrate the anisotropy, have not been computed so far, to the best of our knowledge.

Appendix D: Joint distribution of a_1 and a_2

Let $\tilde{P}(a_1, a_2)$ denote the joint probability distribution of the Brownian functionals

$$a_1 = \int_0^1 B^2(s) ds, \quad \text{and} \quad a_2 = \int_0^1 B(s) ds. \quad (\text{D1})$$

where $B(t)$ is the standard Brownian motion $B(t)$, satisfying $\dot{B}(t) = \eta(t)$, where $\eta(t)$ is a delta-correlated white noise of zero mean. We calculate the double Laplace transform,

$$\begin{aligned} Q(\lambda_1, \lambda_2) &= \langle \exp[-\lambda_1 a_1 - \lambda_2 a_2] \rangle \\ &= \int_0^\infty da_1 \int_{-\infty}^\infty da_2 e^{-\lambda_1 a_1 - \lambda_2 a_2} \tilde{P}(a_1, a_2) \end{aligned} \quad (\text{D2})$$

Using the Brownian path measure, $Q(\lambda_1, \lambda_2)$ can be expressed as a path integral,

$$Q(\lambda_1, \lambda_2) = \int_{-\infty}^\infty dx \int_{B(0)=0}^{B(1)=x} \mathcal{D}B(\tau) \exp \left[-\frac{1}{2} \int_0^1 d\tau \dot{B}^2(\tau) - \lambda_1 \int_0^1 d\tau B^2(\tau) - \lambda_2 \int_0^1 d\tau B(\tau) \right], \quad (\text{D3})$$

where $B(\tau)$ is a Brownian motion that starts at $B(0) = 0$ at time $\tau = 0$ and arrives at a final position $B(1) = x$ at time $\tau = 1$. One then integrates over the final position

x . To evaluate this path integral, we complete the square and rewrite it as follows

$$Q(\lambda_1, \lambda_2) = \int_{-\infty}^{\infty} dx \int_{B(0)=0}^{B(1)=x} \mathcal{D}B(\tau) \exp \left[-\frac{1}{2} \int_0^1 d\tau \dot{B}^2(\tau) - \lambda_1 \int_0^1 d\tau \left\{ \left(B(\tau) + \frac{\lambda_2}{2\lambda_1} \right)^2 - \frac{\lambda_2^2}{4\lambda_1^2} \right\} \right]. \quad (\text{D4})$$

Next, we make a shift $\tilde{B}(\tau) = B(\tau) + \lambda_2/(2\lambda_1)$ and also change $x \rightarrow x + \lambda_2/(2\lambda_1)$. This constant shift does not change the Brownian measure, since $\dot{\tilde{B}}(\tau) = \dot{B}(\tau)$. Hence $\tilde{B}(\tau)$ is another Brownian motion that starts at $\tilde{B}(0) =$

$\lambda_2/(2\lambda_1)$ and arrives at x at $\tau = 1$. For simplicity of notation, we will re-denote $\tilde{B}(\tau)$ as $B(\tau)$ with $B(0) = \lambda_2/(2\lambda_1)$ and $B(1) = x$. Therefore Eq. (D4) can be written as

$$Q(\lambda_1, \lambda_2) = e^{\frac{\lambda_2^2}{4\lambda_1}} \int_{-\infty}^{\infty} dx \int_{B(0)=\lambda_2/(2\lambda_1)}^{B(1)=x} \mathcal{D}B(\tau) \exp \left[-\frac{1}{2} \int_0^1 d\tau \dot{B}^2(\tau) - \lambda_1 \int_0^1 d\tau B^2(\tau) \right]. \quad (\text{D5})$$

The form of the path integral in Eq. (D5) shows immediately that this corresponds to the imaginary time propagator of a quantum harmonic oscillator with Hamiltonian $\hat{H} = -\frac{\hbar^2}{2m} \frac{\partial^2}{\partial x^2} + \frac{1}{2} m \omega^2 x^2$, upon setting $\hbar = m = 1$ and $\omega = \sqrt{2\lambda_1}$. It propagates from the initial position $\lambda_2/(2\lambda_1)$ to the final position x in unit time. Hence we can write

$$Q(\lambda_1, \lambda_2) = e^{\frac{\lambda_2^2}{4\lambda_1}} \int_{-\infty}^{\infty} dx \mathcal{G} \left(x, \frac{\lambda_2}{2\lambda_1}, 1 \right), \quad (\text{D6})$$

where $\mathcal{G}(x, y, t)$ denotes the imaginary time propagator of the quantum harmonic oscillator from the initial position y to the final position x in imaginary time t . This propagator is well-known in the literature [57] and for a given ω , with $\hbar = m = 1$ it reads

$$\mathcal{G}(x, y, t) = \sqrt{\frac{\omega}{2\pi \sinh(\omega t)}} \exp \left[-\frac{\omega}{2 \sinh(\omega t)} [(x^2 + y^2) \cosh(\omega t) - 2xy] \right]. \quad (\text{D7})$$

In our case, setting $\omega = \sqrt{2\lambda_1}$ and $y = \lambda_2/2\lambda_1$, and performing the Gaussian integration over x we finally get

$$Q(\lambda_1, \lambda_2) = \langle \exp[-\lambda_1 a_1 - \lambda_2 a_2] \rangle = \frac{\exp[\lambda_2^2 C(\lambda_1)]}{\sqrt{\cosh(\sqrt{2\lambda_1})}}, \quad (\text{D8})$$

where

$$C(\lambda_1) = \frac{1}{4\lambda_1} \left(1 - \frac{\tanh \sqrt{2\lambda_1}}{\sqrt{2\lambda_1}} \right). \quad (\text{D9})$$

This then provides the derivation of Eq. (8) in the main text. Formally, the joint distribution $\tilde{P}(a_1, a_2)$ can be obtained by inverting the double Laplace transform,

$$\tilde{P}(a_1, a_2) = \int \frac{d\lambda_1}{2\pi i} \int \frac{d\lambda_2}{2\pi i} Q(\lambda_1, \lambda_2) \exp[\lambda_1 a_1 + \lambda_2 a_2]$$

where both integrals are understood as Bromwich integrals for complex λ_1 and λ_2 .

Appendix E: Marginal distribution of $x(t)$

From Eq. (5), we have for time $t \ll D_R^{-1}$

$$x(t) = v_0 t - v_0 D_R t^2 a_1, \quad (\text{E1})$$

where $a_1 = \int_0^1 ds B^2(s)$. Eq. (9) then immediately follows from this relation where $f_x(a_1)$ is the PDF of a_1 . Setting $\lambda_2 = 0$ in Eq. (D8), we get

$$\langle e^{-\lambda_1 a_1} \rangle = \int_0^{\infty} e^{-\lambda_1 a_1} f_x(a_1) da_1 = \frac{1}{\sqrt{\cosh(\sqrt{2\lambda_1})}} \quad (\text{E2})$$

To invert this Laplace transform, we first re-write the right hand side (r.h.s.) as

$$\frac{1}{\sqrt{\cosh(\sqrt{2\lambda_1})}} = \frac{\sqrt{2} e^{-\sqrt{\frac{\lambda_1}{2}}}}{(1 + e^{-2\sqrt{2\lambda_1}})^{1/2}}. \quad (\text{E3})$$

Performing a formal series expansion of Eq. (E3) we get

$$\langle e^{-\lambda_1 a_1} \rangle = \sqrt{2} \sum_{k=0}^{\infty} (-1)^k \frac{(2k)!}{(k!)^2 2^{2k}} e^{-\frac{1}{\sqrt{2}}(1+4k)\sqrt{\lambda_1}}. \quad (\text{E4})$$

We can now invert term by term using the Laplace inversion identity (for $b > 0$)

$$\mathcal{L}_{s \rightarrow x}^{-1} \left[e^{-b\sqrt{s}} \right] = \frac{b}{2\sqrt{\pi x^3}} e^{-\frac{b^2}{4x}}. \quad (\text{E5})$$

This then gives

$$f_x(a_1) = \frac{1}{2\sqrt{\pi a_1^3}} \sum_{k=0}^{\infty} (-1)^k \frac{(4k+1)}{2^{2k}} \binom{2k}{k} e^{-\frac{(4k+1)^2}{8a_1}}, \quad (\text{E6})$$

stated as the formula (11) in the main text. The asymptotic behaviour of $f_x(a_1)$ in the limit $a_1 \rightarrow 0$ is simple to obtain. Indeed, for small a_1 , the series in (E6) is dominated by the $k = 0$ term and we get

$$f_x(a_1) \simeq \frac{1}{2\sqrt{\pi a_1^3}} e^{-\frac{1}{8a_1}}. \quad (\text{E7})$$

Thus the function has an essential singularity as $a_1 \rightarrow 0$. To derive the asymptotic behavior as $a_1 \rightarrow \infty$ turns out to be trickier, as this series representation in Eq. (E6) is not convenient to analyse in that limit. We therefore need a different representation that is well suited for the $a_1 \rightarrow \infty$ limit. To proceed, we use the following identity

$$\frac{1}{\cosh(\sqrt{2\lambda})} = 2 \sum_{n=0}^{\infty} (-1)^n \frac{(n + \frac{1}{2})\pi}{(n + \frac{1}{2})^2 \pi^2 + 2\lambda}, \quad (\text{E8})$$

which can be simply obtained by computing the residues at the zeroes of $\cosh(\sqrt{2\lambda})$ in the complex λ plane. Therefore, we can re-write Eq. (E2) as

$$\int_0^{\infty} e^{-\lambda_1 a_1} f_x(a_1) da_1 = \left[2 \sum_{n=0}^{\infty} \frac{(-1)^n (n + \frac{1}{2})\pi}{(n + \frac{1}{2})^2 \pi^2 + 2\lambda} \right]^{1/2}. \quad (\text{E9})$$

For large a_1 , the dominant contribution comes from the branch-cut around the pole corresponding to the $n = 0$ term in this series (E9). Near this pole, the r.h.s. behaves as $\sqrt{\pi/(\pi^2/4 + 2\lambda)}$. This can be inverted using the identity

$$\mathcal{L}_{\lambda \rightarrow x}^{-1} \left[\frac{1}{\sqrt{\lambda + b}} \right] = \frac{1}{\sqrt{\pi x}} e^{-bx}. \quad (\text{E10})$$

This gives

$$f_x(a_1) \simeq \frac{1}{\sqrt{2a_1}} e^{-\frac{\pi^2}{8} a_1}, \quad (\text{E11})$$

as stated in the main text.

Appendix F: Marginal distribution of $y(t)$

From Eq. (5), we see that

$$y(t) = v_0 \sqrt{2D_R} t^{3/2} a_2, \quad (\text{F1})$$

where $a_2 = \int_0^1 ds B(s)$. This immediately shows that for $t \ll D_R^{-1}$

$$P(y, t) = \frac{1}{v_0 \sqrt{2D_R} t^{3/2}} f_y \left(\frac{y}{v_0 \sqrt{2D_R} t^{3/2}} \right), \quad (\text{F2})$$

where $f_y(a_2)$ is the PDF of $a_2 = \int_0^1 ds B(s)$. The Laplace transform of $f_y(a_2)$ can be obtained by setting $\lambda_1 = 0$ in Eq. (D8). In the limit $\lambda_1 \rightarrow 0$, $C(\lambda_1) \rightarrow 1/6$ in Eq. (D9). Hence we get

$$\langle e^{-\lambda_2 a_2} \rangle = \int_{-\infty}^{\infty} e^{-\lambda_2 a_2} f_y(a_2) da_2 = \exp \left(\frac{\lambda_2^2}{6} \right). \quad (\text{F3})$$

This can be easily inverted to yield a purely Gaussian scaling function

$$f_y(a_2) = \sqrt{\frac{3}{2\pi}} \exp \left(-\frac{3}{2} a_2^2 \right). \quad (\text{F4})$$

This result is stated in the main text, in a slightly different but equivalent form.

Appendix G: Marginal distribution of

$$r^2(t) = x^2(t) + y^2(t)$$

From Eq. (5), we obtain, to leading order for small time $t \ll D_R^{-1}$

$$r^2(t) = x^2(t) + y^2(t) = v_0^2 t^2 - 2v_0^2 D_R t^3 (a_1 - a_2^2), \quad (\text{G1})$$

where $a_1 = \int_0^1 B^2(s) ds$ and $a_2 = \int_0^1 B(s) ds$. This immediately yields the scaling form given in Eq. (12) of the main text where $f_r(z)$ is the PDF of $z = a_1 - a_2^2$. By definition, the distribution of z is thus given by

$$f_r(z) = \int_0^{\infty} da_1 \int_{-\infty}^{\infty} da_2 \tilde{P}(a_1, a_2) \delta(z - (a_1 - a_2^2)), \quad (\text{G2})$$

in terms of the joint PDF of a_1 and a_2 given in Eqs. (D10) and (8). From these equations (D10) and (D8), we notice that the inverse Laplace transform with respect to λ_2 can be performed explicitly, since $Q(\lambda_1, \lambda_2)$ in (D8), as a function of λ_2 , is a pure Gaussian. This yields

$$\tilde{P}(a_1, a_2) = \int \frac{d\lambda_1}{2\pi i} \frac{e^{\lambda_1 a_1}}{\sqrt{\cosh(\sqrt{2\lambda_1})}} \frac{e^{-a_2^2/(4C(\lambda_1))}}{\sqrt{4\pi C(\lambda_1)}}, \quad (\text{G3})$$

where the integral is a Bromwich integral in the complex λ_1 plane. We thus insert this expression (G3) in Eq. (G2) and perform the integral over a_1 (the δ function in Eq. (G2) enforcing $a_1 = z + a_2^2$) and we obtain

$$f_r(z) = \int_{-\infty}^{\infty} da_2 \int \frac{d\lambda_1}{2\pi i} \frac{e^{\lambda_1(z+a_2^2)-a_2^2/(4C(\lambda_1))}}{\sqrt{4\pi \cosh(\sqrt{2\lambda_1}) C(\lambda_1)}}. \quad (\text{G4})$$

The integral over a_2 can now be performed since this is a pure Gaussian integral (provided $\lambda_1 - 1/(4C(\lambda_1)) < 0$, which can be achieved by moving the Bromwich contour) and we obtain

$$f_r(z) = \int \frac{d\lambda_1}{2\pi i} e^{\lambda_1 z} \frac{1}{\sqrt{\cosh(\sqrt{2\lambda_1})}} \frac{1}{\sqrt{1-4\lambda_1 C(\lambda_1)}}. \quad (\text{G5})$$

Finally, using the expression for $C(\lambda_1)$ in Eq. (D9), we have $1 - 4\lambda_1 C(\lambda_1) = \tanh(\sqrt{2\lambda_1})/\sqrt{2\lambda_1}$ and finally Eq. (G5) can be written as (with the change of notation $\lambda_1 \rightarrow \lambda$)

$$f_r(z) = \int \frac{d\lambda}{2\pi i} e^{\lambda z} \left[\frac{\sqrt{2\lambda}}{\sinh \sqrt{2\lambda}} \right]^{1/2}, \quad (\text{G6})$$

which can equivalently be written as

$$\langle e^{-\lambda z} \rangle = \int_0^{\infty} e^{-\lambda z} f_r(z) dz = \left[\frac{\sqrt{2\lambda}}{\sinh(\sqrt{2\lambda})} \right]^{1/2}, \quad (\text{G7})$$

as stated in Eq. (13) in the main text.

We now show how to perform the inverse Laplace transform in the r.h.s. of Eq. (G7) to obtain an explicit expression for $f_r(z)$. We start by re-writing the r.h.s. as

$$\left[\frac{\sqrt{2\lambda}}{\sinh(\sqrt{2\lambda})} \right]^{1/2} = 2^{3/4} \lambda^{1/4} \frac{e^{-\sqrt{\frac{\lambda}{2}}}}{(1 - e^{-2\sqrt{2\lambda}})^{1/2}}. \quad (\text{G8})$$

$$\mathcal{L}_{\lambda \rightarrow x}^{-1} \left(\lambda^{1/4} e^{-b\sqrt{\lambda}} \right) = \frac{\sqrt{b}}{8\sqrt{2\pi}x^{5/2}} e^{-\frac{b^2}{8x}} \left[(b^2 - 2x)K_{1/4} \left(\frac{b^2}{8x} \right) + b^2 K_{3/4} \left(\frac{b^2}{8x} \right) \right], \quad (\text{G13})$$

where $K_\nu(z)$ is the modified Bessel function of index ν . Using this result (G13) for each term in Eq. (G9) we get

$$f_r(z) = \frac{1}{4\pi z^{3/2}} \sum_{k=0}^{\infty} \frac{(2k)!}{(k!)^2 2^{2k}} \sqrt{4k+1} e^{-\frac{(4k+1)^2}{16z}} \left(\left(\frac{(4k+1)^2}{4z} - 1 \right) K_{1/4} \left(\frac{(4k+1)^2}{16z} \right) + \frac{(4k+1)^2}{4z} K_{3/4} \left(\frac{(4k+1)^2}{16z} \right) \right) \quad (\text{G14})$$

Even though this expression is a bit long, it is straightforward to plot this function using Mathematica (indeed the series converges very fast), as shown in Fig. 2(b) in

Performing a formal series expansion of the r.h.s. of Eq. (G8), we obtain

$$\left[\frac{\sqrt{2\lambda}}{\sinh(\sqrt{2\lambda})} \right]^{1/2} = 2^{3/4} \sum_{k=0}^{\infty} \frac{(2k)!}{(k!)^2 2^{2k}} \lambda^{1/4} e^{-\sqrt{\frac{\lambda}{2}}(1+4k)}. \quad (\text{G9})$$

The idea is now to invert the Laplace transform term by term in the r.h.s. of (G9). Each term has the form $h(\lambda) = \lambda^{1/4} e^{-b\sqrt{\lambda}}$ with an appropriate b that depends on k . Hence we need to find the inverse Laplace transform of $h(\lambda)$. This is not completely straightforward. To proceed, we first re-write $h(\lambda)$ as a product of two terms

$$h(\lambda) = \frac{1}{\lambda^{1/4}} \sqrt{\lambda} e^{-b\sqrt{\lambda}}. \quad (\text{G10})$$

The first term $1/\lambda^{1/4}$ can be inverted easily using

$$\mathcal{L}_{\lambda \rightarrow x}^{-1} \left(\frac{1}{\lambda^{1/4}} \right) = \frac{1}{\Gamma(1/4) x^{3/4}}, \quad (\text{G11})$$

and also the term $\sqrt{\lambda} e^{-b\sqrt{\lambda}}$ can be inverted using

$$\mathcal{L}_{\lambda \rightarrow x}^{-1} \left(\sqrt{\lambda} e^{-b\sqrt{\lambda}} \right) = \frac{e^{-\frac{b^2}{4x}} (b^2 - 2x)}{4\sqrt{\pi}x^{5/2}}. \quad (\text{G12})$$

The Laplace transform of the product can then be obtained by the convolution theorem and performing this convolution explicitly, we get

our final expression for the scaling function

the main text.

Asymptotic behaviours of $f_r(z)$: The limit $z \rightarrow 0$ is easy to obtain as it is given by the $k = 0$ term of the series in

Eq. (G14). Using $K_\nu(x) \simeq \sqrt{\pi/(2x)}e^{-x}$ as $x \rightarrow \infty$, we find that the leading order behavior of the $k = 0$ term, and hence that of $f_r(z)$, is given by

$$f_r(z) \simeq \frac{1}{2\sqrt{2\pi}z^2} e^{-\frac{1}{8z}}, \quad \text{as } z \rightarrow 0. \quad (\text{G15})$$

In contrast, the other limit $z \rightarrow \infty$ is trickier as in the case of $f_x(a_1)$ in Eq. (E6). To proceed, it is convenient to go back to the original Laplace transform in Eq. (G7) and re-write its r.h.s. using the following identity

$$\frac{\sqrt{2\lambda}}{\sinh(\sqrt{2\lambda})} = 2 \sum_{n=1}^{\infty} (-1)^{n+1} \frac{n^2 \pi^2}{n^2 \pi^2 + 2\lambda}. \quad (\text{G16})$$

Hence we get from Eq. (G7) the following alternative representation of the Laplace transform which is more suited for the large z analysis of $f_r(z)$

$$\int_0^{\infty} e^{-\lambda z} f_r(z) dz = \left[2 \sum_{n=1}^{\infty} (-1)^{n+1} \frac{n^2 \pi^2}{n^2 \pi^2 + 2\lambda} \right]^{1/2} \quad (\text{G17})$$

For large z , the dominant contribution comes from the branch-cut around the pole corresponding to the $n = 1$ term in this series in Eq. (G17). Near this pole corresponding to $n = 1$, the r.h.s. behaves as $\simeq \pi\sqrt{2}/\sqrt{\pi^2 + 2\lambda}$. Using the identity in Eq. (E10) we obtain

$$f_r(z) \simeq \sqrt{\frac{\pi}{z}} e^{-\frac{\pi^2}{2}z} \quad \text{as } z \rightarrow \infty. \quad (\text{G18})$$

The asymptotic behaviors of $f_r(z)$ in Eqs. (G15) and (G18) have been stated below Eq. (13) in the main text.

-
- [1] P. Romanczuk, M. Bär, W. Ebeling, B. Lindner, and L. Schimansky-Geier, *Eur. Phys. J. Special Topics* **202**, 1 (2012).
- [2] M. C. Marchetti, J. F. Joanny, S. Ramaswamy, T. B. Liverpool, J. Prost, M. Rao, and R. Aditi Simha, *Rev. Mod. Phys.* **85**, 1143 (2013).
- [3] C. Bechinger, R. Di Leonardo, H. Löwen, C. Reichhardt, G. Volpe, and G. Volpe, *Rev. Mod. Phys.* **88**, 045006 (2016).
- [4] S. Ramaswamy, *J. Stat. Mech.* 054002 (2017).
- [5] É. Fodor, and M. C. Marchetti, *Physica A* **504**, 106 (2018).
- [6] F. Schweitzer, *Brownian Agents and Active Particles: Collective Dynamics in the Natural and Social Sciences*, Springer: Complexity, Berlin, (2003).
- [7] *E. Coli in Motion*, H. C. Berg, (Springer Verlag, Heidelberg, Germany) (2004).
- [8] M. E. Cates, *Rep. Prog. Phys.* **75**, 042601 (2012).
- [9] X. Trepat, M. R. Wasserman, T. E. Angelini, E. Millet, D. A. Weitz, J. P. Butler, and J. J. Fredberg, *Nature Physics* **5**, 426 (2009).
- [10] T. Vicsek, A. Czirók, E. Ben-Jacob, I. Cohen, and O. Shochet, *Phys. Rev. Lett.* **75**, 1226 (1995).
- [11] S. Hubbard, P. Babak, S. Th. Sigurdsson, and K. G. Magnússon, *Ecological Modelling*, **174**, 359 (2004).
- [12] D. L. Blair, T. Neicu, and A. Kudrolli, *Phys. Rev. E* **67**, 031303 (2003).
- [13] L. Walsh, C. G. Wagner, S. Schlossberg, C. Olson, A. Baskaran, and N. Menon, *Soft Matter* **13**, 8964 (2017).
- [14] J. Palacci, S. Sacanna, A. P. Steinberg, D. J. Pine, and P. M. Chaikin, *Science* **339**, 936 (2013).
- [15] J. Toner, Y. Tu, and S. Ramaswamy, *Ann. of Phys.* **318**, 170 (2005).
- [16] N. Kumar, H. Soni, S. Ramaswamy, and A. K. Sood, *Nature Comm.* **5**, 4688 (2014).
- [17] Y. Fily, and M. C. Marchetti, *Phys. Rev. Lett.* **108**, 235702 (2012).
- [18] A. B. Slowman, M. R. Evans, and R. A. Blythe, *Phys. Rev. Lett.* **116**, 218101 (2016).
- [19] J. Schwarz-Linek, C. Valeriani, A. Cacciuto, M. E. Cates, D. Marenduzzo, A. N. Morozov, and W. C. K. Poon, *Proc. Natl. Acad. Sci. USA* **109**, 4052 (2012).
- [20] G. S. Redner, M. F. Hagan, and A. Baskaran, *Phys. Rev. Lett.* **110**, 055701 (2013).
- [21] J. Stenhammar, R. Wittkowski, D. Marenduzzo, and M. E. Cates, *Phys. Rev. Lett.* **114**, 018301 (2015).
- [22] A. P. Solon, Y. Fily, A. Baskaran, M. E. Cates, Y. Kafri, M. Kardar, and J. Tailleur, *Nature Physics* **11**, 673 (2015).
- [23] K. Malakar, V. Jemseena, A. Kundu, K. Vijay Kumar, S. Sabhapandit, S. N. Majumdar, S. Redner, and A. Dhar, *J. Stat. Mech.* 043215 (2018).
- [24] U. Erdmann, W. Ebeling, L. Schimansky-Geier, and F. Schweitzer, *Eur. Phys. J. B* **15**, 105 (2000).
- [25] U. Erdmann and W. Ebeling, *Phys. Rev. E* **65**, 061106 (2002).
- [26] J. Tailleur J and M. E. Cates, *Phys. Rev. Lett.* **100**, 218103 (2008).
- [27] J. Tailleur and M. E. Cates, *Euro. Phys. Lett.* **86**, 60002 (2009).
- [28] S. Das, G. Gompper, and R. G Winkler, *New J. Phys.* **20**, 015001 (2018).
- [29] C. Maggi, M. Paoluzzi, N. Pellicciotta, A. Lepore, L. Angelani, R. Di Leonardo, *Phys. Rev. Lett.* **113**, 238303 (2014).
- [30] C. Maggi, U. M. B. Marconi, N. Gnan, and R. Di Leonardo, *Sci. Rep.* **5**, 10742 (2015).
- [31] G. Li and J. X. Tang, *Phys. Rev. Lett.* **103**, 078101 (2009).
- [32] J. Elgeti and G. Gompper, *Euro Phys. Lett.* **109**, 58003 (2015).
- [33] C. G. Wagner, M. F. Hagan and A. Baskaran, *J. Stat. Mech.* 043203 (2017).
- [34] M. E. Cates, and J. Tailleur, *Europhys. Lett.* **101**, 20010

- (2013).
- [35] A. Pototsky, and H. Stark, *Europhys. Lett.* **98**, 50004 (2012).
- [36] A. P. Solon, M. E. Cates, and J. Tailleur, *Eur. Phys. J. Special Topics* **224**, 1231 (2015).
- [37] D. Mumford, in *Algebraic geometry and its applications* (pp. 491-506), Springer, New York (1994).
- [38] D. Gredat, I. Dornic, and J. M. Luck, *J. Phys. A: Math. Theor.* **44**, 175003 (2011).
- [39] J. R. Howse, R. A. L. Jones, A. J. Ryan, T. Gough, R. Vafabakhsh, and R. Golestanian, *Phys. Rev. Lett.* **99**, 048102 (2007).
- [40] F. J. Sevilla, and L. A. Gómez Nava, *Phys. Rev. E* **90**, 022130 (2014).
- [41] S. N. Majumdar, *Curr. Sci.* **77**, 370 (1999).
- [42] A. J. Bray, S. N. Majumdar, and G. Schehr, *Adv. in Phys.* **62**, 225 (2013).
- [43] T. W. Burkhardt, *J. Stat. Mech.* P07004 (2007).
- [44] T. W. Burkhardt, *First Passage of a Randomly Accelerated Particle in First-Passage Phenomena and Their Applications*, edited by R. Metzler, G. Oshanin, and S. Redner (World Scientific, 2014).
- [45] J. Masoliver and K. G. Wang, *Phys. Rev. E* **51**, 2987 (1995).
- [46] T. W. Burkhardt, *J. Phys. A: Math. Gen.* **26**, L1157 (1993).
- [47] S. N. Majumdar, A. Rosso, and A. Zoia, *J. Phys. A: Math. Theor.* **43**, 115001 (2010).
- [48] S. N. Majumdar, *Current Science* **89**, 2076 (2005).
- [49] F. J. Sevilla and M. Sandoval, *Phys. Rev. E* **91**, 052150 (2015).
- [50] C. Kurzthaler, C. Devailly, J. Arlt, T. Franosch, W. C. Poon, V. A. Martinez, and A. T. Brown, *Phys. Rev. Lett.* **121**, 078001 (2018).
- [51] L. Angelani, R. Di Lionardo, and M. Paoluzzi, *Euro. J. Phys. E* **37**, 59 (2014).
- [52] A. Scacchi and A. Sharma, *Mol. Phys.* **116**, 460 (2017).
- [53] T. Demaerel and C. Maes, *Phys. Rev. E* **97**, 032604 (2018).
- [54] S. Redner, *A Guide to First-Passage Processes*, Cambridge University Press (2001).
- [55] U. Basu, S. N. Majumdar, A. Rosso, and G. Schehr, in preparation.
- [56] S. C. Takatori, R. De Dier, J. Vermant, and J. F. Brady, *Nature Comm.* **7**, 10694 (2016).
- [57] R. P. Feynman, A. R. Hibbs, *Quantum Mechanics and Path Integrals*, (McGraw- Hill, New York, 1965).
- [58] O. Dauchot, and V. Démery, preprint arXiv:1810.13303.